NeuroImage 245 (2021) 118743

Contents lists available at ScienceDirect

NeuroImage

journal homepage: www.elsevier.com/locate/neuroimage

Gene expression associated with individual variability in intrinsic functional connectivity

Liangfang Li[a], Yongbin Wei[b], Jinbo Zhang[a], Junji Ma[a], Yangyang Yi[a], Yue Gu[a], Liman Man Wai Li[c], Ying Lin[a], Zhengjia Dai[a,*]

[a] Department of Psychology, Sun Yat-sen University, Guangzhou 510006, China
[b] Department of Complex Trait Genetics, Center for Neurogenomics and Cognitive Research, Amsterdam Neuroscience, Vrije Universiteit Amsterdam, Amsterdam, Netherlands
[c] Department of Psychology and Centre for Psychosocial Health, The Education University of Hong Kong, Hong Kong SAR, China

ARTICLE INFO

Keywords:
Intersubject variability
Functional connectivity
Resting-state fMRI
Gene expression
Metabolism

ABSTRACT

It has been revealed that intersubject variability (ISV) in intrinsic functional connectivity (FC) is associated with a wide variety of cognitive and behavioral performances. However, the underlying organizational principle of ISV in FC and its related gene transcriptional profiles remain unclear. Using resting-state fMRI data from the Human Connectome Project (299 adult participants) and microarray gene expression data from the Allen Human Brain Atlas, we conducted a transcription-neuroimaging association study to investigate the spatial configurations of ISV in intrinsic FC and their associations with spatial gene transcriptional profiles. We found that the multimodal association cortices showed the greatest ISV in FC, while the unimodal cortices and subcortical areas showed the least ISV. Importantly, partial least squares regression analysis revealed that the transcriptional profiles of genes associated with human accelerated regions (HARs) could explain 31.29% of the variation in the spatial distribution of ISV in FC. The top-related genes in the transcriptional profiles were enriched for the development of the central nervous system, neurogenesis and the cellular components of synapse. Moreover, we observed that the effect of gene expression profile on the heterogeneous distribution of ISV in FC was significantly mediated by the cerebral blood flow configuration. These findings highlighted the spatial arrangement of ISV in FC and their coupling with variations in transcriptional profiles and cerebral blood flow supply.

1. Introduction

Intersubject variability (ISV) in the functional connectivity (FC) of the human brain underlies individual differences in cognition and behavior (Finn and Todd Constable, 2016; Kelly et al., 2012; Smith et al., 2015). Recently, resting-state fMRI (R-fMRI) studies suggested that the ISV in intrinsic FC exhibited a sizeable regional variation for both adults (Li et al., 2019; Mueller et al., 2013) and neonates (Gao et al., 2014; Stoecklein et al., 2020), with higher ISV in multimodal association cortices than in unimodal cortices. These regions with high ISV in FC can not only predict individual differences in higher-order cognitive functions (e.g., inhibition and fluid intelligence) but also provide valuable information for individual identification (Finn et al., 2015; Horien et al., 2019; Liu et al., 2018). Moreover, previous works demonstrated that the overall spatial pattern of ISV in FC detected in the neonatal brain was similar to the spatial distribution observed in healthy adults (Gao et al., 2014; Stoecklein et al., 2020). The similar overall spatial distribution of ISV in FC between the neonatal brain and the adult brain highlighted the effect of gene expression on the spatial distribution of ISV in FC. Moreover, human twin studies have suggested that the FC is heritable (Anderson et al., 2021; Ge et al., 2017; Glahn et al., 2010; Miranda-Dominguez et al., 2018). The similarity in FC was greater for monozygotic twins relative to dizygotic twins and unrelated individuals. However, the mechanism underlying the contribution of genetic factors to the heterogeneous distribution of ISV in FC remains poorly understood.

Previous studies have begun to explore the genetic basis of human brain FC organization (Gao et al., 2014; Richiardi et al., 2015; Vértes et al., 2016; Wang et al., 2015). In the study of Gao et al. (2014), the genetic contribution to ISV in FC was estimated by comparing FC variability across monozygotic twins, dizygotic twins and unrelated singleton pairs. They found that an increased degree of genetic sharing (100% in monozygotic twins) was significantly associated with a decrease in FC variability, which indicated a strong genetic effect on ISV in FC. However, the previous study on the genetic contribution to ISV in FC mainly revealed the high heritability of FC, and which genes are associated with the heterogeneous distribution of ISV in FC remains unknown. Doan et al. (2016) identified human accelerated regions (HARs)

* Corresponding author.
E-mail address: daizhengj@mail.sysu.edu.cn (Z. Dai).

https://doi.org/10.1016/j.neuroimage.2021.118743.
Received 20 May 2021; Received in revised form 28 October 2021; Accepted 16 November 2021
Available online 17 November 2021.

of the human genome, which represented genomic loci with accelerated divergence in humans compared to other species using the comparative genome analysis. Genes located in human accelerated regions, labeled as HAR genes, have been found to relate to neuron development processes, such as cortical expansion, neurogenesis, and neuronal differentiation (Doan et al., 2016; Wei et al., 2019; Won et al., 2019), and regulate human-specific social and behavioral traits (Doan et al., 2016). Notably, the effect of HAR genes involved in various functions across the entire human body, which is not specific to the brain. Wei et al. (2019) then identified a set of HAR genes, labeled as HAR-BRAIN genes, by overlapping HAR genes set with BRAIN genes set, which were characterized as significantly higher expressed in brain sites than non-brain sites. They found that HAR-BRAIN genes played a crucial role in the cortical expansion and cortical organization of cognitive functional networks in the human brain. Recent research suggested that cortical expansion has been considered to be an influential factor affecting the heterogeneous distribution of ISV (Mueller et al., 2013; Stoecklein et al., 2020). Therefore, we speculated that the regional variation in gene expression profile of HAR-BRAIN genes would be a potential genetic underpinning of the heterogeneous distribution of ISV in FC. However, how the gene expression profile shapes the heterogeneous distribution of ISV in FC remains largely unknown.

The regions with high ISV in FC, which are primarily located in the prefrontal and parietal cortices, largely overlap with the regions with high cerebral blood flow (Liang et al., 2013). Resting-state cerebral blood flow (CBF) reflects the regional metabolism level and is a fundamental physiological property of the human brain (Satterthwaite et al., 2014). Moreover, resting-state CBF is also influenced by genetic factors that are involved in neurogenesis and neuron development (Goyal et al., 2014). In addition, a previous study has found that the genes that influence brain metabolism also regulate FC (Glahn et al., 2010). Hence, we speculated that the brain metabolism level might mediate the effect of gene expression on ISV in FC.

To uncover the mechanism underlying the contributions of genetic factors to ISV in FC, we conducted a transcription-neuroimaging association study (Fig. 1 for schematic of this study). Our first aim was to investigate the spatial configurations of ISV in FC based on high-resolution R-fMRI data from the Human Connectome Project (HCP; 299 adult participants) (Van Essen et al., 2013) and their relationship to a variety of cognitive abilities based on the meta-analysis method of the NeuroSynth database (Yarkoni et al., 2011). Based on previous studies (Gao et al., 2014; Mueller et al., 2013), we hypothesized that the high ISV in FC would be located in the association cortices, which tend to be responsible for higher-order functions. Our second aim was to investigate the relationship between gene expression profiles obtained from the Allen Human Brain Atlas (Hawrylycz et al., 2012) and intersubject variability in FC by directly examining the overlapping spatial variations of gene expression profiles and ISV in FC. We hypothesized that the expression of HAR-BRAIN genes, which are crucial for brain neuron development, would significantly correlate with ISV in FC. Our third aim was to examine the potential mediation effect of resting-state CBF by conducting a mediation analysis to model the relationships among the gene expression profile, CBF, and the spatial distribution of ISV in FC.

2. Materials and methods

2.1. Participants

Data of 339 unrelated healthy adults from the released dataset of 900 participants were obtained from the Human Connectome Project (HCP; Van Essen et al., 2013). Since the HCP provides data from a large number of twins and non-twin siblings, we only selected unrelated participants, each with a unique family ID, to avoid confounding effects induced by shared genetic and environmental factors within a family structure. All participants were between 22 and 37 years old and had provided written informed content. The HCP project was approved by the Institutional Review Board of Washington University in St. Louis.

2.2. R-fMRI data acquisition

All R-fMRI data were collected using a customized 32-channel Siemens 3T Connectome Skyra scanner. During scanning, the participants were asked to open their eyes, stare at the bright cross-hair on a black background, and relax. The R-fMRI data were collected in two sessions on two different days. Each session consisted of two run scans with a left-to-right (LR) and a right-to-left (RL) phase encoding direction, resulting in 4 resting-state run scans for each participant. Each R-fMRI run was acquired using a multiband gradient-echo-planar imaging sequence as follows: time repetition (TR) = 720 ms, time echo (TE) = 33.1 ms, flip angle = 52°, field of view = 208×180 mm^2, matrix = 104×90, 72 slices, voxel size = 2×2×2 mm^3, multiband factor = 8, and 1200 volumes (scanning time: 14.4 min). To eliminate the potential impact of different phase encoding directions on our findings, our analyses were restricted to the R-fMRI data with LR phase-encoding runs in two different sessions.

2.3. R-fMRI data preprocessing

The R-fMRI data were first preprocessed by the HCP according to the HCP minimal preprocessing procedure (Glasser et al., 2013), which included gradient distortion correction, head motion correction, image distortion correction, spatial transformation to the Montreal Neurological Institute (MNI) space, and intensity normalization. Forty participants were discarded due to excessive head motion in either session with the exclusion criteria of mean frame-wise head motion above 0.14 mm (filename: Movement_RelativeRMS_mean.txt) (Finn et al., 2015). Therefore, 299 participants (28.46±3.69 years old, 139 male/160 female) were used for subsequent analyses. Further data preprocessing conducted by the current study was performed using the Data Processing Assistant for Resting-State fMRI (DPARSF) (Yan and Zang, 2010; Yan et al., 2016) and Statistical Parametric Mapping software (SPM12; http://fil.ion.ucl.ac.uk/spm). These additional preprocessing steps we performed included: (1) removing linear trend; (2) regressing out nuisance signals [including 24 head motion parameters (Friston et al., 1996), cerebrospinal fluid, white matter and global signals (Birn et al., 2006; Fox et al., 2009)]; and (3) performing temporal bandpass filtering (0.01–0.1 Hz). The residuals were used to construct FC matrix.

2.4. FC matrix construction

To construct the whole-brain FC matrix, the parcellation atlas with 625 similar-sized regions was used to parcellate the brain gray matter (excluding cerebellum) into 625 regions of interest (ROIs), which preserved the automated anatomical labeling (AAL) landmarks (Dai et al., 2019; Tzourio-Mazoyer et al., 2002; Zalesky et al., 2010). The time series were then extracted from each ROI by averaging the time series of all voxels within that region. Finally, the Pearson's correlation coefficients between the time courses of each possible pair of ROIs were calculated and normalized using Fisher's z-transformation, resulting in a 625×625 FC matrix for each participant.

2.5. ISV in FC

ROI-level ISV. To derive the spatial distribution map of ISV in FC across the whole brain, we calculated the ISV in FC pattern based on each ROI (Fig. 1). The FC map of each ROI was denoted as a 624-dimensional real vector $F_i(s, t)$, where $i \in \{1, 2, \ldots, 625\}$, $s \in \{1, 2, \ldots, 299\}$, $t \in \{1, 2\}$ indicated the respective indices of ROIs, participants, and scan sessions, and each element corresponded to the FC between ROI i and the remaining 624 ROIs. Given an ROI i and a participant s,

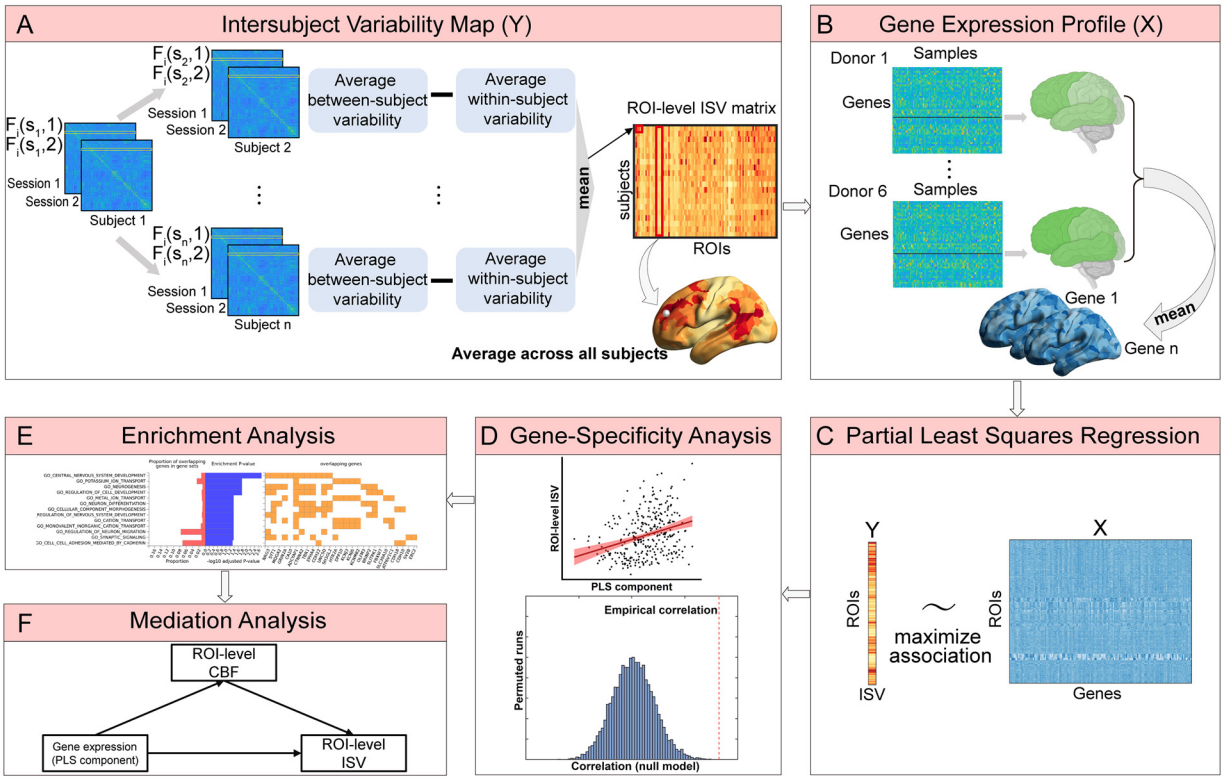

Fig. 1. Schematic diagram of study design and methodology. (A) Using the repeat-measured R-fMRI data from HCP to calculate the ROI-level ISV in FC. (B) Using the microarray gene expression data across cortical regions from the Allen Human Brain Atlas to obtain the average gene expression profiles across six donors. (C) Using the partial least squares regression to investigate the association between the distribution of ISV in FC and gene expression profiles. (D) Gene-specificity analysis of ISV-related transcription-neuroimaging associations. (E) Gene enrichment analysis for top-related genes. (F) Mediation analysis for testing the relationships between the genes, resting-state CBF and ISV in FC. ISV, intersubject variability; FC, functional connectivity; PLS, partial least squares; CBF, cerebral blood flow.

the within-subject variability in ROI-level FC between two sessions was quantified as

$$V_i^{\mathrm{W}}(s) = 1 - corr\big(F_i(s,1),\ F_i(s,2)\big), \tag{1}$$

where $corr$ was the function of the Pearson's correlation. The average within-subject variability of two different participants s_1 and s_2 for ROI i was defined as

$$MV_i^{\mathrm{W}}(s_1,s_2) = \frac{1}{2}\left[V_i^{\mathrm{W}}(s_1) + V_i^{\mathrm{W}}(s_2)\right]. \tag{2}$$

In addition to the within-subject variability, the between-subject variability between s_1 and s_2 for ROI i in each scan session was estimated as

$$V_i^{\mathrm{B}}(s_1,s_2,t) = 1 - corr\big(F_i(s_1,t),\ F_i(s_2,t)\big). \tag{3}$$

The average between-subject variability of two different participants across two sessions for ROI i was defined as

$$MV_i^{\mathrm{B}}(s_1,s_2) = \frac{1}{2}\left[V_i^{\mathrm{B}}(s_1,s_2,1) + V_i^{\mathrm{B}}(s_1,s_2,2)\right]. \tag{4}$$

Based on the above definitions, we defined the intersubject variability (ISV) of ROI i between two different participants s_1 and s_2 by removing the average within-subject variability $MV_i^{\mathrm{W}}(s_1,s_2)$ from the average between-subject variability $MV_i^{\mathrm{B}}(s_1,s_2)$, i.e.,

$$ISV_i(s_1,s_2) = MV_i^{\mathrm{B}}(s_1,s_2) - MV_i^{\mathrm{W}}(s_1,s_2). \tag{5}$$

The intersubject variability $ISV_i(s)$ of an ROI i regarding a single participant s was then calculated as the mean of the intersubject variabilities between s and the other 298 participants. By averaging the intersubject variabilities across all of the participants, we obtained the average ISV of ROI i as follows:

$$ISV_i = \frac{1}{299}\sum_{s=1}^{299} ISV_i(s). \tag{6}$$

Finally, we repeated the above computation for all 625 ROIs, resulting in a 625×1 ISV map.

Within-module-level ISV. To quantify the ISV in FC at the modular level, the 625 ROIs were partitioned into seven functional modules (Yeo et al., 2011), including the visual (Vis), somatomotor (Mot), dorsal attention (dATN), ventral attention (vATN), limbic (LMB), frontoparietal (FPN), and default mode network (DMN). In particular, each ROI was assigned to the module that had the maximum number of voxels overlapping with the ROI. Notably, 19 ROIs in the subcortical region were not involved in the construction of the within-module FC maps because they did not overlap with any of the above modules. For each module, we first extracted the FC values between all pairs of ROIs within the module to produce the within-module FC maps. Then, the ISV of the within-module FC patterns was calculated in a similar way as that of the above ROI-level ISV, except that the FC map of each ROI was replaced by the within-module FC map (for more details, please refer to the Supplementary materials). As such, we obtained a 299×7 within-module-level ISV matrix, in which each element was the mean of the intersubject variabilities between a single participant and the other 298 participants within the related module.

To compare the mean within-module-level ISV difference between different modules, a nonparametric permutation test (N = 10,000) was performed. The false discovery rate (FDR) correction was adopted for multiple comparisons with a significance threshold of $p < 0.05$.

2.6. Behavioral data

To investigate the mechanism of how the regional ISV in FC underlies previously observed individual differences in specific behavior and cognition, a NeuroSynth meta-analysis was implemented to assess behavioral topics associated with regional ISV using the NeuroSynth meta-

analytic database (http://www.neurosynth.org) (Yarkoni et al., 2011). Specifically, the original ISV map was split into 20 intervals with five-percentile increments (i.e., intervals from 0-5% to 95-100%) and then binarized to obtain 20 binary maps. Each of the 20 binary maps was used as an input to the meta-analysis, and the outputs of the analysis were z-statistics associated with the 23 behavioral topics representing a wide range of behaviors (e.g., motor, emotion, and working memory) (Margulies et al., 2016; Preti and Van De Ville, 2019). NeuroSynth meta-analysis could provide additional insights into detailed differences in ISV composition patterns of the brain regions involved in different cognitive functions.

2.7. Gene expression

2.7.1. AHBA dataset

To characterize the genetic underpinnings of ISV in FC, the gene symbol list of 415 brain-expressed HAR genes (further referred to as HAR-BRAIN genes) was first obtained from Wei et al. (2019), and the gene expression profiles of these HAR-BRAIN genes were extracted from the complete microarray gene expression data from the Allen Human Brain Atlas dataset (AHBA) (http://human.brain-map.org/static/download) (Hawrylycz et al., 2012). AHBA consists of expression profiles of 20,700 genes measured by 58,692 probes for 3702 spatially distinct tissue samples collected from the postmortem brains of six human donors (all without a history of neuropsychiatric or neuropathological disorders) (for details, see Table S1 and Supplementary materials). Tissue samples of the left hemisphere were included in this study, as data from all six donors were available for the left hemisphere, and only two donors were available for the right hemisphere. The local gene expression values of each sample were accompanied by the X, Y, and Z coordinates in MNI152 space indicating where the samples were extracted, allowing us to map expression values to other brain atlas.

After obtaining the gene expression values and the MNI152 coordinates for each sample from AHBA, we adapted a data-reduction and mapping procedure similar to that of Wei et al. (2019) and Romme et al. (2017) to map the gene expression values of tissue samples in AHBA to brain regions of AAL-625 atlas. First, for each donor, expression values from multiple probes corresponding to the same gene were averaged to generate 20,700 gene expression levels for each sample, according to the instructions in the Probe.csv of each donor's microarray data files. Further, gene expression values of all genes on each sample were normalized by dividing by the average gene expression value of the sample. Second, samples outside the left hemisphere were excluded according to the sample annotation in SampleAnnot.csv of each donor's microarray data files. Third, we calculated the minimal Euclidean distance between the reported MNI coordinates of samples and the MNI coordinates of all gray matter voxels located in the left hemisphere of the AAL-625 atlas to find the closest voxel for each sample. Each sample was assigned to a particular ROI to which the closest voxel belonged, and a distance threshold of 2 mm was used to eliminate the inaccurate assignment of ROI. We checked the assignment by visual examination to ensure that the location of the sample overlapped with that of the assigned ROI. After performing the above procedure, tissue samples of six donors were spatially mapped to 302 ROIs.

The gene expression data were computed for each ROI by averaging the expression data of the samples mapped to that particular ROI. Gene expression data of each gene were normalized to z-scores across all ROIs in each donor's dataset. Normalized gene expression data were then averaged across six donors to obtain a 302×20,700 group-level gene expression matrix. Gene expression data of 415 HAR-BRAIN genes were extracted from the complete group-level gene expression data matrix, resulting in a 302×415 HAR-BRAIN gene expression matrix. To investigate whether the HAR-BRAIN genes were more highly expressed particularly in the modules with high within-module-level ISV (e.g., FPN, DMN, dATN), the HAR-BRAIN gene expression matrix was first averaged across genes to obtain the average gene expression for each ROI and then averaged within each of the seven functional modules. A non-parametric permutation test ($N = 10{,}000$) was performed to compare the mean gene expression difference between modules with FDR for multiple comparisons correction.

2.8. Relationship among ISV in FC, HAR-BRAIN gene expression, and CBF

2.8.1. Correlation between ISV map and HAR-BRAIN gene expression profile

To test our hypothesis that the HAR-BRAIN gene expression may be a genetic root of the heterogeneous distribution of ISV in FC, we used partial least squares (PLS) regression to identify the expression patterns of HAR-BRAIN genes that were significantly correlated with ISV in FC. PLS regression is a multivariate analysis aiming to identify the components, which were linear combinations of the weighted gene expression scores (predictor variables), that were the most predictive to ISV in FC (response variables). PLS regression has been widely used for neuroimaging and transcriptional data analyses (Liu et al., 2020; Morgan et al., 2019; Seidlitz et al., 2018; Vértes et al., 2016; Whitaker et al., 2016). Here, we used the code shared by Whitaker et al. (2016) to conduct the PLS regression.

To examine whether the real R^2 of the component that explained more than 10% of the total variance (Liu et al., 2020) was significantly larger than that achieved by chance, we permutated 10,000 spatial-autocorrelation-preserving surrogate maps using the generative modeling implemented in BrainSMASH software (Brain Surrogate Maps with Autocorrelated Spatial Heterogeneity, Burt et al., 2020) to generate the R^2 null model for PLS regression. The reason for generating spatial-autocorrelation-preserving surrogate map rather than completely random map was to alleviate the confounding effect driven by spatial autocorrelation structure, which is a ubiquitous property of spatially embedded brain data, and to capture the transcriptomic-neuroimaging association that cannot be solely attributed to general spatial trends (Burt et al., 2020; Fornito et al., 2019; Markello and Misic, 2021). We also used a similar permutation test with spatial autocorrelation controlled to examine the significance of the empirical spatial correlation between PLS components and the ROI-level ISV map. Moreover, to determine whether the HAR-BRAIN genes were more specifically associated with the ISV map than the other genes, we conducted two types of gene-specificity analyses. Specifically, we randomly selected equal number of HAR-BRAIN genes (i.e., 415 genes) from the pool of 2564 BRAIN genes (excluding HAR-BRAIN genes, type I) and 20,285 AHBA genes (excluding HAR-BRAIN genes, type II) to repeat the PLS regression for 10,000 times, respectively. The BRAIN genes featuring as significantly more expressed in brain tissues compared to other available body sites were obtained from Wei et al. (2019). The Spearman's correlations between the PLS components and the ISV map obtained from 10,000 repetitions constituted two null models (type I and type II). Furthermore, we used the bootstrapping method to estimate the error in the estimation of the weight of each gene and divided the weight of each gene by the estimated error to generate the corrected weight. We ranked the genes according to their corrected weights, which represented their contributions to the PLS component.

To identify the possible biological functions of ISV-related genes, in line with prior studies (Anderson et al., 2020), we performed gene-category enrichment analysis (GCEA) for the top-ranked related genes with positive weight (top 10%) in the first few significant components by using the SBP-spatial ensemble null model implemented in a recently released toolbox (Fulcher et al., 2021). Compared with randomizing gene-to-category assignments, SBP-spatial ensemble null model utilizes an ensemble of phenotypes with a given spatial autocorrelation structure, preserving the properties of the gene expression data (e.g., within-category gene coexpression and similar spatial autocorrelation structure) and the spatial autocorrelation characteristic of the original phenotype simultaneously, which may help to build a more conservative spatially constrained null distribution to reduce the false positive

rate (Fulcher et al., 2021). Specifically, we used the Gene Ontology (GO) term hierarchy files (data version 2019–04–17) and corresponding annotation files for Homo sapiens (goa_human.gaf), which were downloaded from the Gene Ontology Resource (Ashburner et al., 2000) on April 17, 2019 (Fulcher et al., 2021) to examine whether the top-ranked related genes were enriched for the predefined GO categories that have specific functional interpretations in three functional categories, including biological process, cellular component, and molecular function. According to the pipeline of the GCEA toolbox, we completed the gene-to-category annotations and preprocessed the hierarchy relationships between GO categories, and further restricted our analysis to GO categories with 10–200 gene annotations (Fulcher et al., 2021). For each GO category, we simulated 10,000 spatially autocorrelated surrogate ISV maps using the BrainSMASH software (Burt et al., 2020) to constitute the null model to test the significance of category-level gene score, which was measured as the average spatial correlation between ISV map and gene expression profile of multiple genes within the category. The *p*-values were estimated after fitting the Gaussian distribution to the estimated null distribution and the resulting *p*-values were corrected across GO categories through FDR with $p < 0.05$. The GO categories with an FDR *p*-value below 0.05 were reported.

2.8.2. Correlation between ISV map and the CBF map

To explore whether the spatial distribution of ISV in FC can reflect the CBF configuration, we compared the spatial distributions of the ISV map and those of the CBF map in the resting state, which shows the brain regions' metabolic costs (Satterthwaite et al., 2014). Specifically, according to the MNI coordinates of the voxels within each ROI, the blood flow values of the corresponding coordinates were extracted from the CBF map and averaged to obtain an ROI-level CBF map based on the AAL-625 atlas. Notably, we deleted 12 ROIs in which the blood flow values of more than 90% of voxels within that ROI were zeros. Then, we calculated the spatial correlation between the ROI-level ISV map and CBF map and performed spatial-autocorrelation-preserving permutation test to examine the significance of the empirical spatial correlation.

2.8.3. Mediation analysis

To test the hypothesis that the CBF distribution mediated the contribution of the gene expression profile to the ISV map, a bootstrapped mediation analysis was performed using the simple mediation model (model 4) from the PROCESS macro in SPSS (Hayes, 2017). The mediation analysis was conducted with 5000 bootstrap samples to generate bias-corrected confidence intervals (CI). The indirect effect was considered significant when the bootstrapped 95% CI did not include zero (Hayes, 2017).

3. Results

3.1. Spatial distribution of ISV in FC across brain regions and intrinsic modules

We observed that the spatial distribution of ISV in FC [measured by Eq. (6)] was regionally heterogeneous (Fig. 2A). The association cortices, including the prefrontal (dorsolateral superior frontal gyrus, middle frontal gyrus, inferior frontal gyrus), temporal (middle temporal gyrus, superior temporal gyrus), and parietal lobe (supramarginal gyrus), showed high ISV. Meanwhile, the unimodal cortices, including the primary visual (cuneus, lingual gyrus, superior occipital gyrus), sensorimotor (postcentral gyrus, precentral gyrus), and subcortical areas (pallidum, caudate nucleus, thalamus, amygdala) showed low ISV. This pattern was compatible with previous observations of individual variability in FC (Mueller et al., 2013).

For within-module-level ISV, visual inspection indicated that higher-order cognitive modules, including FPN and dATN, had the highest variability, whereas LMB and the primary modules, including the Vis and Mot, had the lowest variability (Fig. 2B) (for details, see Table S2). The permutation test revealed that the ISV of the four higher-order cognitive modules (FPN, dATN, DMN, vATN) was significantly higher than that of LMB and the primary modules (Vis, Mot) (*p*s < 0.035, 10,000 permutations, FDR corrected). In addition, the ISV of vATN was significantly lower than that of FPN and dATN (*p*s < 0.024, 10,000 permutations, FDR corrected) (for details, see Table S3).

3.2. Spatial distribution of ISV in FC reflected a cognitive spectrum from primary to higher-order functions

By overlapping the 20 binary ISV maps with the 23 behavioral topic maps available from the NeuroSynth database, we found that low-ISV regions were more related to primary functions, such as "motor", "multisensory processing", and "auditory processing", and high-ISV regions were related to higher-order functions, such as "language", "cognitive control", "working memory", "numerical cognition" and "inhibition" (Fig. 2C). The behavior of the topics arranged from bottom to top corresponded to the function of the modules in Fig. 2B that was sorted according to the within-module-level ISV.

3.3. Expression profile of HAR-BRAIN genes across brain regions and intrinsic modules

To investigate how the spatial distribution of ISV in FC was related to the expression of 415 HAR-BRAIN genes, we mapped the samples in the AHBA dataset to the ROIs, and estimated the average expression of 415 HAR-BRAIN genes for each ROI. HAR-BRAIN genes showed high-level expression in regions of the frontal cortices (medial superior frontal gyrus, orbital superior frontal gyrus, dorsolateral superior frontal gyrus), temporal pole (superior temporal gyrus, middle temporal gyrus), and anterior cingulate and paracingulate gyri. Meanwhile, the visual cortices (fusiform gyrus, lingual gyrus) and subcortical regions (thalamus, pallidum, parahippocampal gyrus, caudate nucleus, putamen) displayed low-level gene expression (Fig. 3A). Hence, there was an overall tendency that the average expression of HAR-BRAIN genes increased from subcortical regions and primary areas to the association cortices.

The permutation test indicated that the HAR-BRAIN genes showed significantly higher expression levels in LMB, DMN, dATN, vATN, and FPN than in Vis (*p*s < 0.024, 10,000 permutations, FDR corrected), but no significant difference was detected among these five modules (for details, see Table S4 and S5). In addition, the gene expression in the DMN was significantly higher than that in the Mot ($p = 0.024$, 10,000 permutations, FDR corrected) (Fig. 3B).

3.4. Gene expression profile was associated with the spatial distribution of ISV in FC

Using PLS regression, we found that two significant components explained 31.29% of the variance in ISV ($p < 0.001$, permutation tests with spatial autocorrelation corrected, 10,000 permutations) (Fig. S1 and S2). Specifically, the first partial least squares component (PLS1) represented a significantly positive association between ISV in FC and a gene expression profile characterized by high expression mainly in the prefrontal, parietal, and lateral temporal areas (Spearman's $\rho = 0.532$, $p = 0.0004$, permutation tests with spatial autocorrelation corrected, 10,000 permutations) (Fig. 3C, 3D). The second independent partial least squares component (PLS2) also represented a significantly positive association between ISV in FC and a gene expression profile displaying high expression predominantly in the subcortical, temporal and prefrontal areas (Spearman's $\rho = 0.432$, $p = 0.0011$, permutation tests with spatial autocorrelation corrected, 10,000 permutations) (Fig. 3F, 3G). The results of type I gene-specificity analysis showed that the Spearman's correlation between PLS1, PLS2, and ISV in FC was significantly higher than that of the null model (PLS1: $p < 0.001$; PLS2: $p = 0.0167$), which was based on equally sized random gene sets taken from BRAIN genes (Fig. 3E, 3H). The type II gene-specificity analysis

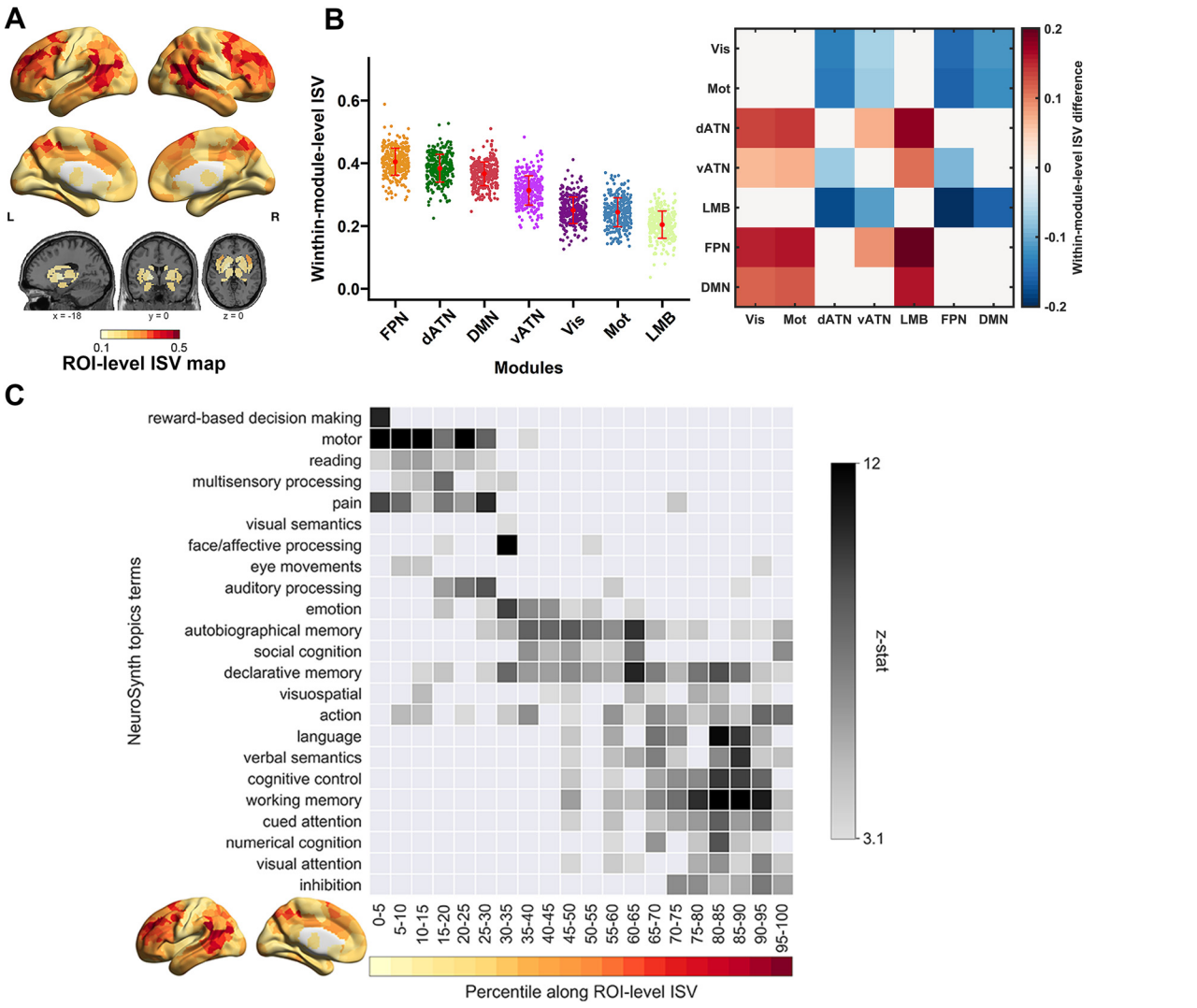

Fig. 2. Spatial distribution map of ISV in FC and results of NeuroSynth meta-analysis. (A) Spatial distribution of ROI-level ISV. The subcortical regions displayed in Fig. 2 and 3 included insula, caudate, putamen, pallidum, thalamus, hippocampus, and amygdala. (B) Comparison of within-module-level ISV. The error bar indicates the standard deviation (SD) of the within-module-level ISV across all the participants under each module. The matrix on the right shows the within-module-level ISV differences between the modules (row-column); within-module-level ISV differences that are not significant in the permutation test ($p > 0.05$) are set to zeros. (C) NeuroSynth meta-analysis of regions of interest along the ISV using 23 behavioral topic terms. Terms are ordered by the weighted mean z-statistics of their location along the ISV. ISV, intersubject variability; FC, functional connectivity.

based on the AHBA gene pool found that the Spearman's correlation between PLS1 and ISV remained significantly higher than that of the null model ($p = 0.0078$) (Fig. S3A), while the association between PLS2 and ISV was no longer significant ($p = 0.2613$) (Fig. S3B). These findings suggested that the spatial expression pattern of PLS1 component played a specific role in shaping the spatial distribution of ISV in FC.

The GCEA results showed that the transcriptional profile of PLS1 component was significantly enriched in GO categories related to the biological processes involved in central nervous system development, regulation of cell development, neurogenesis, neuron differentiation and metabolic process ($ps < 0.05$, FDR corrected), and the transcriptional profile of PLS1 component was significantly enriched in GO categories associated with the cellular components of the synapse, synaptic membrane, plasma membrane (integral component and intrinsic component), and cell junction ($ps < 0.05$, FDR corrected). Moreover, the transcriptional profile of PLS1 component was also significantly enriched in GO categories related to the molecular function such as protein binding and ion binding ($ps < 0.05$, FDR corrected). Meanwhile, the GCEA results of the transcriptional profile derived from PLS2 component were similar to that of PLS1 component ($ps < 0.05$, FDR corrected). Detailed results of GCEA, which included the significant GO category name, gene symbol, category scores, original and corrected *p*-values, were tabulated in Supplemental Table 1–6 (Supplemental Table 1–3 for PLS1 and 4–6 for PLS2).

3.5. CBF mediated the association between the gene expression profile and ISV in FC

As reported by Satterthwaite et al. (2014), brain CBF varied regionally in the resting state, with high CBF primarily distributed in the bilateral dorsolateral prefrontal cortex, superior and medial frontal cortex, posterior cingulate cortex, lateral temporal cortex and inferior parietal lobes (Fig. 4A). A significant positive correlation was shown between the CBF and ISV in FC (Spearman's $\rho = 0.336$, $p = 0.0034$, permutation tests with spatial autocorrelation corrected, 10,000 permutations) (Fig. 4B). Additionally, we found that higher gene expression of PLS1 was associated with higher CBF (path a: $\beta = 0.313$, $p < 0.001$). After controlling the influence of PLS1, higher CBF was related to higher ISV

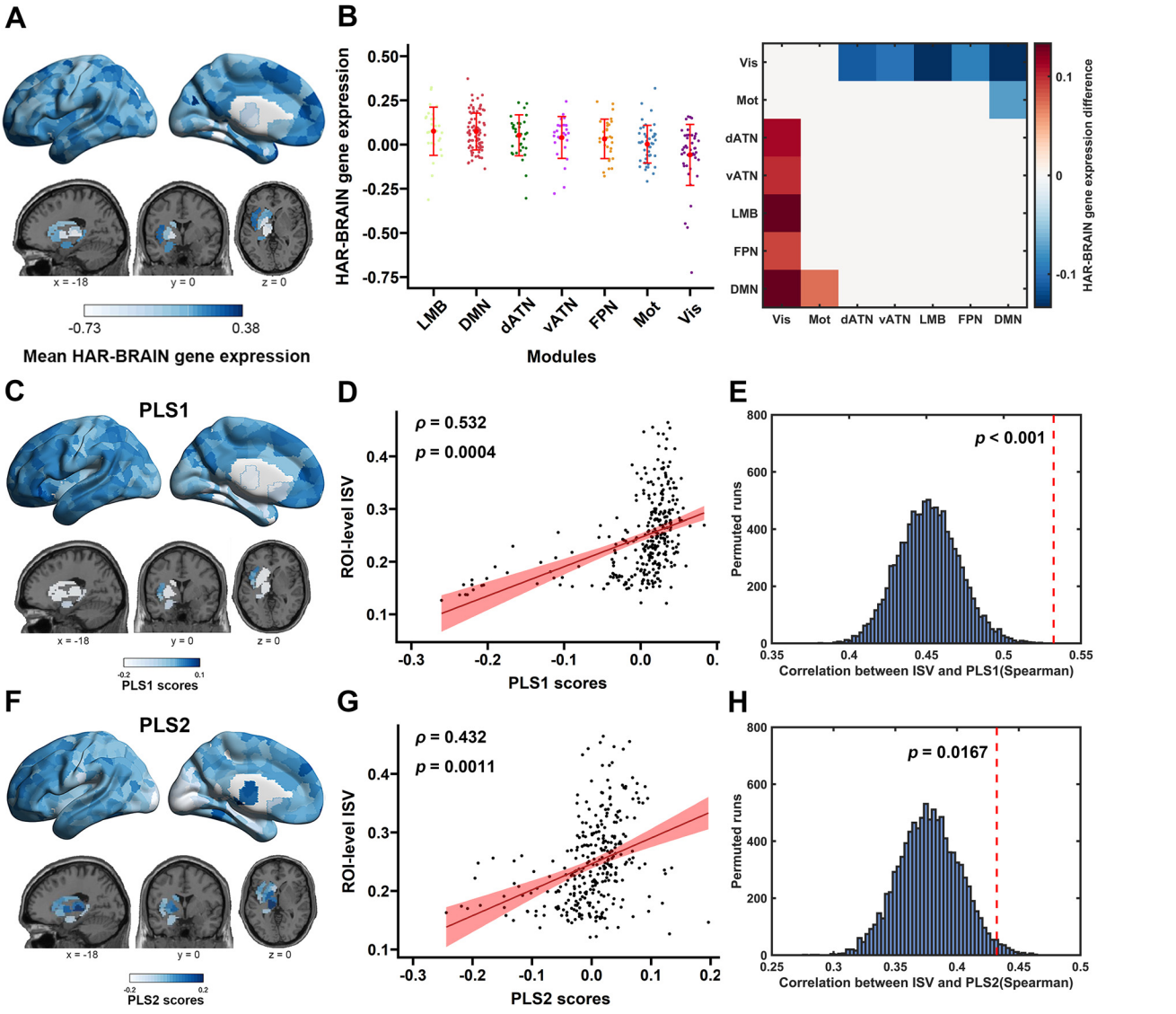

Fig. 3. Association between gene expression profiles and ISV in FC. (A) Average expression profile of HAR-BRAIN genes. (B) HAR-BRAIN gene expression within each module ranked in the descending order of the mean gene expression. The error bar indicates the SD of the average gene expression levels of ROIs within the same module. The matrix on the right shows the gene expression differences between the modules (row-column); gene expression differences that are not significant in the permutation test ($p > 0.05$) are set to zeros. (C) PLS1 identifies a gene expression profile with overexpression mainly in the prefrontal, parietal and lateral temporal cortices. (D) Spearman's correlation between PLS1 and ROI-level ISV in FC. Spatial correlation was tested for significance against a spatial-autocorrelation-preserving null distribution (BrainSMASH). The red shadow indicates the 95% CI. (E) Gene-specificity analysis of the association between PLS1 and ROI-level ISV in FC. The red dotted line represents the empirical correlation value. (F) PLS2 identifies a gene expression profile with overexpression dominantly in the subcortical, temporal and prefrontal cortices. (G) Spearman's correlation between PLS2 and ROI-level ISV in FC. Spatial correlation was tested for significance against a spatial-autocorrelation-preserving null distribution (BrainSMASH). (H) Gene-specificity analysis of the association between PLS2 and ROI-level ISV in FC. ISV, intersubject variability; FC, functional connectivity; PLS1, the first partial least squares regression component; PLS2, the second partial least squares regression component.

(path b: $\beta = 0.201$, $p < 0.001$). After considering the effect of CBF, the effect of PLS1 on ISV was weakened (path c': $\beta = 0.378$, $p < 0.001$, from path c: $\beta = 0.441$, $p < 0.001$). Furthermore, mediation analysis revealed that CBF was a significant mediator (indirect effect = 0.063, 95% CI = [0.031, 0.104]), partially explaining the positive association between PLS1 and ISV (Fig. 4C, top), while CBF did not mediate the positive association between PLS2 and ISV (indirect effect = 0.019, 95% CI = [−0.008, 0.050]) (Fig. 4C, bottom).

4. Discussion

Using R-fMRI, gene expression, and CBF data, we showed that the changes in the human genome during evolution played an important role in shaping the distribution of ISV in FC. First, we found that ISV in FC distributed heterogeneously across the whole brain, showing greater ISV in multimodal association cortices whilst less ISV in unimodal cortices and subcortical areas. Additionally, we found that the spatial distribution of ISV in FC reflected a cognitive spectrum from primary to higher-order functions using a NeuroSynth meta-analysis. Second, we demonstrated that the spatial distribution of ISV in FC was correlated with the transcriptional profiles of HAR-BRAIN genes across regions, and the most correlated genes were related to the development of synapses and the central nervous system, neurogenesis, and neuron differentiation. Finally, we revealed that the effect of the gene expression profile on the heterogeneous distribution of ISV in FC was significantly mediated by the CBF configuration. Together, these findings may enhance our understanding of the molecular and neural mechanisms associated with the spatial arrangement of ISV in FC.

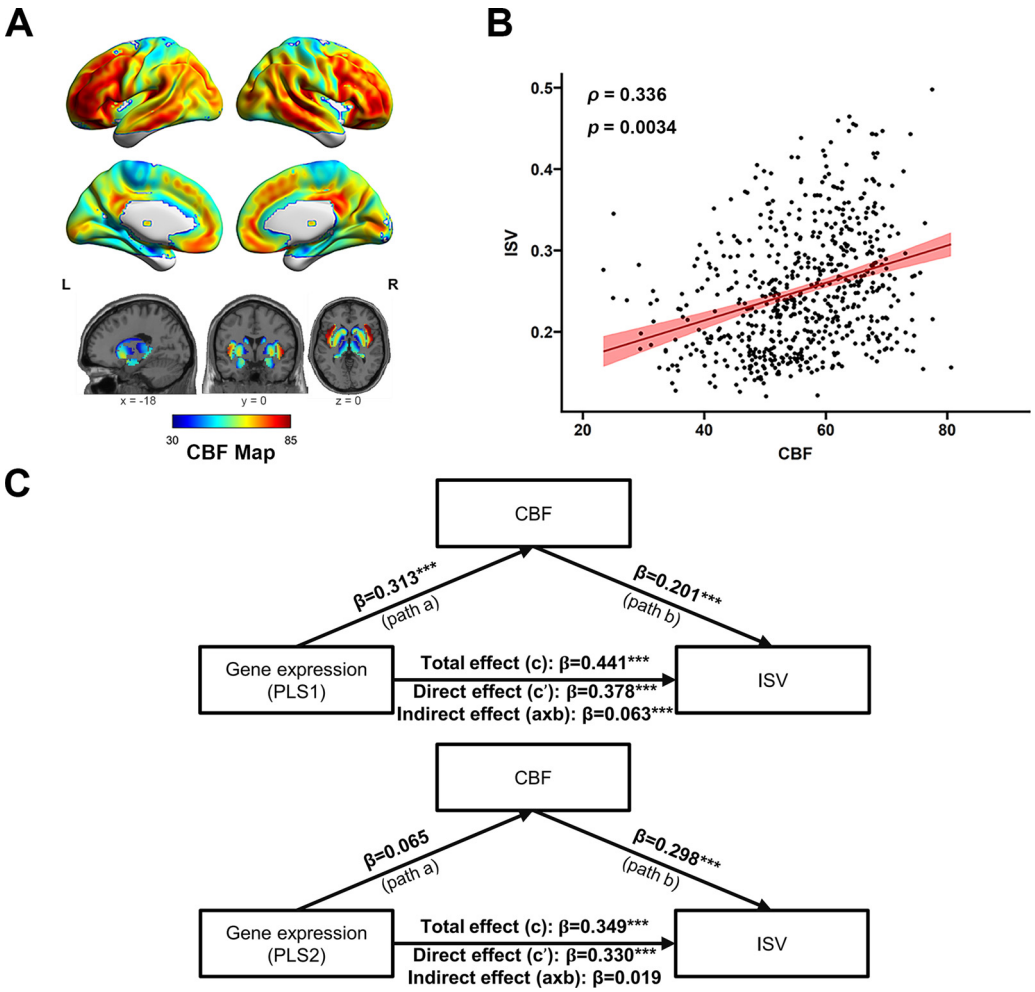

Fig. 4. The CBF map and mediation analysis. (A) CBF map extracted from Satterthwaite et al. (2014). (B) Spearman's correlation between ROI-level CBF and ROI-level ISV. ROI-level CBF was calculated as the average CBF of all voxels within each ROI. Notably, we deleted 12 ROIs in which the blood flow values of more than 90% of voxels within that ROI were zeros. The red shadow indicates the 95% CI. Spatial correlation was tested for significance against a spatial-autocorrelation-preserving null distribution (BrainSMASH) (C) The relationship between gene expression profiles of PLS1 (top) and ISV in FC was mediated by CBF. Standardized regression coefficients were reported. CBF, cerebral blood flow; ISV, intersubject variability; PLS1, the first partial least squares regression component; PLS2, the second partial least squares regression component. $^{***}p < 0.001$.

4.1. Spatial distribution of ISV in FC

The overall pattern of ISV in FC observed in healthy young adults was comparable with the distribution observed in healthy elderly people (Mueller et al., 2013) and in infants (Gao et al., 2014; Stoecklein et al., 2020), suggesting that the overall pattern of ISV in FC may be consistent across different age groups. Previous studies have consistently found that the spatial distribution of ISV in FC emerges during infancy (Gao et al., 2014; Stoecklein et al., 2020), which may reveal the contribution of genetic influences to ISV in FC. In addition, when comparing the pattern of ISV in FC of the neonate brain with that of the adult brain, the association cortices demonstrated a marked increment of ISV in FC for adults, which reflected that postnatal environmental and developmental factors were likely to contribute to ISV in FC (Stoecklein et al., 2020). These results suggest that the genes and environment shape the ISV in FC together. In addition, previous studies have shown that association cortices expanded dramatically during human brain evolution, while the primary cortices showed small cortical expansion (Ardesch et al., 2019; Buckner and Krienen, 2013). The association cortices also expanded more during postnatal development and matured more slowly (Buckner and Krienen, 2013; Hill et al., 2010; Tau and Peterson, 2010), which may make the association cortices more susceptible to developmental environments, such as education, leading to the observed high variability in FC. The function of primary cortices may tend to be similar across individuals since the primary cortices need to be relatively mature in early life to support early survival, such as supporting functions like vision and movement (Lin et al., 2008; Smyser et al., 2010), making postnatal environment less influential on primary cortices. Notably, we found that the limbic system exhibited the lowest variability among all functional modules, which was inconsistent with its moderate variability observed in a previous study (Fig. 2B; Mueller et al., 2013). The discrepancy may be caused by different sample ages. Although the spatial distribution of ISV detected in different age groups was similar in the overall pattern, which demonstrated greater ISV in multimodal association cortices and less ISV in unimodal regions (Gao et al., 2014; Ma et al., 2021; Stoecklein et al., 2020), there are still some differences in the ISV values across different age groups. For example, the multimodal association cortices of adult brain demonstrated a marked increase in variability compared with infant brain, which was thought to result from more interactions between gene expression and environment over a longer period of time (Gao et al., 2014; Stoecklein et al., 2020). Meanwhile, a recent study

found that the individual variability in FC of the subcortical network, which has a strong regional overlapping with the limbic system, increased significantly with age, although it was still lower than that in the association cortices (Ma et al., 2021). Further, they found that compared with other functional networks, the individual variability in FC of the subcortical network was relatively low in adults, while relatively high in the elderly. Hence, it may be reasonable that our findings based on young people (28 years old) were different from those based on older people (52 years old) (Mueller et al., 2013), and further study is needed to depict the development curve of ISV in FC across the lifespan.

4.2. Expression of synapse and neuron development-related genes was associated with ISV in FC

We found that the expression profiles of the genes related to human brain evolution (HAR-BRAIN genes) were positively correlated with the spatial distribution of ISV in FC. In other words, HAR-BRAIN genes were more highly expressed in the association cortices than in the unimodal cortices, leading to an overall trend of higher gene expression in higher-order cognitive modules than in primary modules, which was in accordance with previous work done by Wei et al. (2019). The expression of HAR-BRAIN genes is known to be involved in the evolutionary cortical expansion of the human brain (Wei et al., 2019), which is considered a potential cause of ISV in FC (Mueller et al., 2013; Wang and Liu, 2014). These findings suggested that the expression profiles of HAR-BRAIN genes played an important role in shaping the distribution of ISV in FC, which may be achieved by shaping the evolutionary cortical expansion of the human brain.

Moreover, we found that the HAR-BRAIN genes, which were highly associated with ISV in FC, were significantly enriched for genes involved in synapse development, development of the central nervous system, neurogenesis, neuron differentiation and metabolic process. Previous studies have demonstrated that neurogenesis and neuron differentiation are critical processes in the generation and development of neurons in the human brain (Ming and Song, 2011), suggesting that HAR-BRAIN genes may affect ISV in FC by regulating neuron development and synaptic pruning. In the gene-category enrichment analysis on the top 10% PLS1 genes, we observed some common HAR-BRAIN genes associated with human brain development. For example, ADCYAP1 modulates dendritic spine maturation and morphogenesis (Hayata-Takano et al., 2019), CDH10 is essential in managing the ratio of excitatory and inhibitory synapses on dendrites (Batool et al., 2019), and CTNNA2 is widely expressed in the central nervous system and is critical for synaptic plasticity and brain morphogenesis (Terracciano et al., 2011). These findings also suggested that HAR-BRAIN genes may influence ISV in FC by involving synaptogenesis and synaptic plasticity.

We found that both the spatial variation of gene expression and that of ISV followed a global spatial gradient, extending from primary sensorimotor cortices to higher-order association areas, which was consistent with the well-known processing hierarchy of the human brain (for review, see Huntenburg et al., 2018). To examine the potential role of cortical hierarchy, we conducted a mediation analysis with the principal gradient scores sourced from Margulies et al. (2016) as the mediator. Results indicated that the principal gradient partially mediated the positive association between the gene expression pattern of PLS component and ISV map (please refer to Supplementary materials and Fig. S4). When we controlled the influence of the principal gradient, the effect of gene expression pattern on ISV distribution was weakened but remained significant, which suggested that the relationship between gene expression and ISV may exist beyond broad spatial gradient. Previous studies have consistently found that brain-wide gene expression profile follows hierarchical gradients (Burt et al., 2018; Fornito et al., 2019; Hawrylycz et al., 2012). Moreover, the hierarchical gradient was considered to reflect a gradual increase in the degree to which stimuli undergo multisensory integration, suggesting that individual differences were more likely to occur in advanced cognitive integration processes, rather than in primary cognitive processes.

In the type II gene-specificity analysis based on 20,285 AHBA genes, the correlation between PLS2 gene expression pattern and ISV distribution was no longer significant, suggesting that the gene expression pattern of PLS2 component may not be specifically related to ISV distribution, but was driven by the general genome-wide expression pattern. Hence, we suggest caution when interpreting the findings of PLS2 gene expression pattern. Notably, the spatial correlations between PLS1 gene expression profile and ISV map were both significantly higher than that of BRAIN genes and AHBA genes, which highlighted the specific role of PLS1 component in shaping the spatial pattern of ISV.

4.3. CBF map mediated the positive association between the gene expression profiles and ISV in FC

We found that CBF partially mediated the positive association between the gene expression profiles of HAR-BRAIN genes and ISV in FC. In other words, the brain regions with high levels of HAR-BRAIN gene expression tended to receive more CBF and induce high ISV in FC. The regions with high-level gene expression were mainly distributed in the association cortices, which largely overlapped with the brain regions with high CBF (Liang et al., 2013). Combining the results of gene enrichment analysis and mediation analysis, we speculated that the high-level gene expression in association cortices might drive the generation of a greater number of synapses and more complex synapse connectivity architecture (Goyal and Raichle, 2013). To support the normal development of synapses and their neural activity in these regions, more blood flow is required to provide nutrient supplies such as oxygen and glucose. Moreover, a previous study found that the spatial variation in CBF was positively associated with gene expression profiles related to synapse formation and growth (Goyal et al., 2014; Richiardi et al., 2015), which is consistent with our results. Moreover, CBF can influence the formation of FC. The fluctuation of CBF among individuals may result in ISV in FC patterns, especially in the association cortices. The association cortices with high CBF had a higher demand for metabolism and energy consumption, which may make them more vulnerable to fluctuations in CBF among different individuals and insufficient blood supply (Crossley et al., 2014). On the other hand, as mentioned above, CBF plays an important role in synaptic development, so fluctuations in CBF among individuals may also lead to individual differences in brain development (Paniukov et al., 2020; Satterthwaite et al., 2014), especially in association cortices where the developmental time course is longer than that of primary cortices. These studies provide support for our finding that brain CBF plays a role in mediating the relationship between the gene expression profile and the heterogeneous distribution of ISV in FC.

5. Limitations

Several limitations of the current study should be considered. First, the gene expression data from the AHBA were sampled from six donors who had different ethnicities and sexes. This limited sample might have created a bias in capturing the spatial variation in gene expression profile. However, AHBA is currently the only publicly available database that can provide high-resolution brain-wide mRNA gene expression data. In the future, larger samples containing brain-wide genome-wide gene expression data are needed to obtain a more reliable spatial pattern of gene expression profile and verify our findings. Moreover, future research could explore the relationship between the inter-individual variability of regional gene expression and regional ISV in FC based on larger samples containing brain-wide genome-wide gene expression data. Second, considering that the gene expression map and ISV map are both calculated based on adult samples and the correlational method was used in the current study, there are limitations in establishing causal molecular mechanisms of the ISV pattern. The current study could be

regarded as a preliminary study to explore the relationships between the gene expression profile, CBF, and ISV in FC based on spatial similarity. Third, the currently reported variability map was constructed based on the imaging data of living participants, while the gene expression data were derived from postmortem brains, and the CBF map was constructed based on another dataset. Therefore, the results may be influenced by differences among the datasets, making it difficult to capture the relationship among the gene expression profile, CBF, and ISV in FC at the individual level. Future studies could implement individual-level genome-wide analysis and metabolic data to help further understand the genetic and physiological basis underlying ISV in FC.

Declaration of Competing Interest

None

Acknowledgement

Funding: This work was supported by the National Natural Science Foundation of China (NSFC) (No. 61772569, 71701219), the Guangdong Basic and Applied Basic Research Foundation (No. 2019A1515012148), and the Fundamental Research Funds for the Central Universities (No. 19wkzd20).

Data of the current study were provided by a public dataset Human Connectome Project (HCP). HCP funding was provided by the National Institute of Dental and Craniofacial Research (NIDCR), the National Institute of Mental Health (NIMH), and the National Institute of Neurological Disorders and Stroke (NINDS). HCP data are disseminated by the Laboratory of Neuro Imaging at the University of Southern California.

Author contributions

Conceptualization: Liangfang Li, Yongbin Wei, Zhengjia Dai; **Formal analysis**: Liangfang Li, Jinbo Zhang; **Funding acquisition**: Zhengjia Dai; **Investigation**: Liangfang Li, Junji Ma, Yangyang Yi; **Methodology**: Liangfang Li, Yongbin Wei, Jinbo Zhang, Zhengjia Dai; **Writing – original draft**: Liangfang Li, Zhengjia Dai; **Writing – review & editing**: Liangfang Li, Yongbin Wei, Jinbo Zhang, Junji Ma, Yangyang Yi, Yue Gu, Liman Man Wai Li, Ying Lin, Zhengjia Dai.

Ethics statement

Data of the current study were obtained from a public dataset Human Connectome Project (HCP). The HCP project was approved by the Institutional Review Board of Washington University in St. Louis. All participants had provided written informed content.

Data and code availability statement

The HCP data is publicly available in the database of Human Connectome Project: https://db.humanconnectome.org/data/projects/HCP_1200. The microarray gene expression data is publicly available in Allen Human Brain Atlas dataset: http://human.brain-map.org/static/download. The cerebral blood flow map can be obtained from Satterthwaite et al. (2014). We also uploaded de-identified FC matrices of available participants (https://zenodo.org/record/5607652) in the present study. Detailed documented code for measures calculation, statistical analysis, and figure generation was available with this article (https://github.com/LiangfangLi/ISVGeneExpression).

Supplementary materials

Supplementary material associated with this article can be found, in the online version, at doi:10.1016/j.neuroimage.2021.118743.

References

Anderson, K.M., Collins, M.A., Kong, R., Fang, K., Li, J., He, T., Chekroud, A.M., Yeo, B.T.T., Holmes, A.J., 2020. Convergent molecular, cellular, and cortical neuroimaging signatures of major depressive disorder. Proc. Natl. Acad. Sci. 117, 25138–25149. doi:10.1073/pnas.2008004117.

Anderson, K.M., Ge, T., Kong, R., Patrick, L.M., Spreng, R.N., Sabuncu, M.R., Yeo, B.T.T., Holmes, A.J., 2021. Heritability of individualized cortical network topography. Proc. Natl. Acad. Sci. 118. doi:10.1073/pnas.2016271118.

Ardesch, D.J., Scholtens, L.H., Li, L., Preuss, T.M., Rilling, J.K., Heuvel, M.P.van den, 2019. Evolutionary expansion of connectivity between multimodal association areas in the human brain compared with chimpanzees. Proc. Natl. Acad. Sci. 116, 7101–7106. doi:10.1073/pnas.1818512116.

Ashburner, M., Ball, C.A., Blake, J.A., Botstein, D., Butler, H., Cherry, J.M., Davis, A.P., Dolinski, K., Dwight, S.S., Eppig, J.T., Harris, M.A., Hill, D.P., Issel-Tarver, L., Kasarskis, A., Lewis, S., Matese, J.C., Richardson, J.E., Ringwald, M., Rubin, G.M., Sherlock, G., 2000. Gene ontology: tool for the unification of biology. Nat. Genet. 25, 25–29. doi:10.1038/75556.

Batool, S., Raza, H., Zaidi, J., Riaz, S., Hasan, S., Syed, N.I., 2019. Synapse formation: from cellular and molecular mechanisms to neurodevelopmental and neurodegenerative disorders. J. Neurophysiol. 121, 1381–1397. doi:10.1152/jn.00833.2018.

Birn, R.M., Diamond, J.B., Smith, M.A., Bandettini, P.A., 2006. Separating respiratory-variation-related fluctuations from neuronal-activity-related fluctuations in fMRI. Neuroimage 31, 1536–1548. doi:10.1016/j.neuroimage.2006.02.048.

Buckner, R.L., Krienen, F.M., 2013. The evolution of distributed association networks in the human brain. Trends Cogn. Sci. 17, 648–665. doi:10.1016/j.tics.2013.09.017.

Burt, J.B., Demirtaş, M., Eckner, W.J., Navejar, N.M., Ji, J.L., Martin, W.J., Bernacchia, A., Anticevic, A., Murray, J.D., 2018. Hierarchy of transcriptomic specialization across human cortex captured by structural neuroimaging topography. Nat. Neurosci. 21, 1251–1259. doi:10.1038/s41593-018-0195-0.

Burt, J.B., Helmer, M., Shinn, M., Anticevic, A., Murray, J.D., 2020. Generative modeling of brain maps with spatial autocorrelation. Neuroimage 220, 117038. doi:10.1016/j.neuroimage.2020.117038.

Crossley, N.A., Mechelli, A., Scott, J., Carletti, F., Fox, P.T., McGuire, P., Bullmore, E.T., 2014. The hubs of the human connectome are generally implicated in the anatomy of brain disorders. Brain 137, 2382–2395. doi:10.1093/brain/awu132.

Dai, Z., Lin, Q., Li, T., Wang, X., Yuan, H., Yu, X., He, Y., Wang, H., 2019. Disrupted structural and functional brain networks in Alzheimer's disease. Neurobiol. Aging 75, 71–82. doi:10.1016/j.neurobiolaging.2018.11.005.

Doan, R.N., Bae, B.-I., Cubelos, B., Chang, C., Hossain, A.A., Al-Saad, S., Mukaddes, N.M., Oner, O., Al-Saffar, M., Balkhy, S., Gascon, G.G., Nieto, M., Walsh, C.A., 2016. Mutations in human accelerated regions disrupt cognition and social behaviour. Cell 167, 341–354.e12. doi:10.1016/j.cell.2016.08.071, e12.

Finn, E.S., Shen, X., Scheinost, D., Rosenberg, M.D., Huang, J., Chun, M.M., Papademetris, X., Constable, R.T., 2015. Functional connectome fingerprinting: identifying individuals using patterns of brain connectivity. Nat. Neurosci. 18, 1664–1671. doi:10.1038/nn.4135.

Finn, E.S., Todd Constable, R., 2016. Individual variation in functional brain connectivity: implications for personalized approaches to psychiatric disease. Dialogues Clin. Neurosci. 18, 277–287. doi:10.31887/dcns.2016.18.3/efinn.

Fornito, A., Arnatkevičiūtė, A., Fulcher, B.D., 2019. Bridging the gap between connectome and transcriptome. Trends Cogn. Sci. 23, 34–50. doi:10.1016/j.tics.2018.10.005.

Fox, M.D., Zhang, D., Snyder, A.Z., Raichle, M.E., 2009. The global signal and observed anticorrelated resting state brain networks. J. Neurophysiol. 101, 3270–3283. doi:10.1152/jn.90777.2008.

Friston, K.J., Williams, S., Howard, R., Frackowiak, R.S., Turner, R., 1996. Movement-related effects in fMRI time-series. Magn. Reson. Med. 35, 346–355. doi:10.1002/mrm.1910350312.

Fulcher, B.D., Arnatkeviciute, A., Fornito, A., 2021. Overcoming false-positive gene-category enrichment in the analysis of spatially resolved transcriptomic brain atlas data. Nat. Commun. 12, 2669. doi:10.1038/s41467-021-22862-1.

Gao, W., Elton, A., Zhu, H., Alcauter, S., Smith, J.K., Gilmore, J.H., Lin, W., 2014. Intersubject variability of and genetic effects on the brain's functional connectivity during infancy. J. Neurosci. 34, 11288–11296. doi:10.1523/JNEUROSCI.5072-13.2014.

Ge, T., Holmes, A.J., Buckner, R.L., Smoller, J.W., Sabuncu, M.R., 2017. Heritability analysis with repeat measurements and its application to resting-state functional connectivity. Proc. Natl. Acad. Sci. 114, 5521–5526. doi:10.1073/pnas.1700765114.

Glahn, D.C., Winkler, A.M., Kochunov, P., Almasy, L., Duggirala, R., Carless, M.A., Curran, J.C., Olvera, R.L., Laird, A.R., Smith, S.M., Beckmann, C.F., Fox, P.T., Blangero, J., 2010. Genetic control over the resting brain. Proc. Natl. Acad. Sci. 107, 1223–1228. doi:10.1073/pnas.0909969107.

Glasser, M.F., Sotiropoulos, S.N., Wilson, J.A., Coalson, T.S., Fischl, B., Andersson, J.L., Xu, J., Jbabdi, S., Webster, M., Polimeni, J.R., Van Essen, D.C., Jenkinson, M., WU-Minn HCP Consortium, 2013. The minimal preprocessing pipelines for the Human Connectome Project. Neuroimage 80, 105–124. doi:10.1016/j.neuroimage.2013.04.127.

Goyal, M.S., Hawrylycz, M., Miller, J.A., Snyder, A.Z., Raichle, M.E., 2014. Aerobic glycolysis in the human brain is associated with development and neotenous gene expression. Cell Metab. 19, 49–57. doi:10.1016/j.cmet.2013.11.020.

Goyal, M.S., Raichle, M.E., 2013. Gene expression-based modeling of human cortical synaptic density. Proc. Natl. Acad. Sci. 110, 6571–6576. doi:10.1073/pnas.1303453110.

Hawrylycz, M.J., Lein, E.S., Guillozet-Bongaarts, A.L., Shen, E.H., Ng, L., Miller, J.A., van de Lagemaat, L.N., Smith, K.A., Ebbert, A., Riley, Z.L., Abajian, C., Beckmann, C.F., Bernard, A., Bertagnolli, D., Boe, A.F., Cartagena, P.M., Chakravarty, M.M., Chapin, M., Chong, J., Dalley, R.A., Daly, B.D., Dang, C., Datta, S., Dee, N., Dol-

beare, T.A., Faber, V., Feng, D., Fowler, D.R., Goldy, J., Gregor, B.W., Haradon, Z., Haynor, D.R., Hohmann, J.G., Horvath, S., Howard, R.E., Jeromin, A., Jochim, J.M., Kinnunen, M., Lau, C., Lazarz, E.T., Lee, C., Lemon, T.A., Li, L., Li, Y., Morris, J.A., Overly, C.C., Parker, P.D., Parry, S.E., Reding, M., Royall, J.J., Schulkin, J., Sequeira, P.A., Slaughterbeck, C.R., Smith, S.C., Sodt, A.J., Sunkin, S.M., Swanson, B.E., Vawter, M.P., Williams, D., Wohnoutka, P., Zielke, H.R., Geschwind, D.H., Hof, P.R., Smith, S.M., Koch, C., Grant, S.G.N., Jones, A.R., 2012. An anatomically comprehensive atlas of the adult human brain transcriptome. Nature 489, 391–399. doi:10.1038/nature11405.

Hayata-Takano, A., Kamo, T., Kijima, H., Seiriki, K., Ogata, K., Ago, Y., Nakazawa, T., Shintani, Y., Higashino, K., Nagayasu, K., Shintani, N., Kasai, A., Waschek, J.A., Hashimoto, H., 2019. Pituitary adenylate cyclase-activating polypeptide modulates dendritic spine maturation and morphogenesis via microRNA-132 upregulation. J. Neurosci. 39, 4208–4220. doi:10.1523/JNEUROSCI.2468-18.2019.

Hayes, A.F., 2017. Introduction to Mediation, Moderation, and Conditional Process Analysis: A regression-Based Approach. Guilford publications.

Hill, J., Inder, T., Neil, J., Dierker, D., Harwell, J., Essen, D.V., 2010. Similar patterns of cortical expansion during human development and evolution. Proc. Natl. Acad. Sci. 107, 13135–13140. doi:10.1073/pnas.1001229107.

Horien, C., Shen, X., Scheinost, D., Constable, R.T., 2019. The individual functional connectome is unique and stable over months to years. Neuroimage 189, 676–687. doi:10.1016/j.neuroimage.2019.02.002.

Huntenburg, J.M., Bazin, P.-L., Margulies, D.S., 2018. Large-scale gradients in human cortical organization. Trends Cogn. Sci. 22, 21–31. doi:10.1016/j.tics.2017.11.002.

Kelly, C., Biswal, B.B., Craddock, R.C., Castellanos, F.X., Milham, M.P., 2012. Characterizing variation in the functional connectome: promise and pitfalls. Trends Cogn. Sci. 16, 181–188. doi:10.1016/j.tics.2012.02.001.

Li, M., Wang, D., Ren, J., Langs, G., Stoecklein, S., Brennan, B.P., Lu, J., Chen, H., Liu, H., 2019. Performing group-level functional image analyses based on homologous functional regions mapped in individuals. PLOS Biol 17, e2007032. doi:10.1371/journal.pbio.2007032.

Liang, X., Zou, Q., He, Y., Yang, Y., 2013. Coupling of functional connectivity and regional cerebral blood flow reveals a physiological basis for network hubs of the human brain. Proc. Natl. Acad. Sci. 110, 1929–1934. doi:10.1073/pnas.1214900110.

Lin, W., Zhu, Q., Gao, W., Chen, Y., Toh, C.-.H., Styner, M., Gerig, G., Smith, J.K., Biswal, B., Gilmore, J.H., 2008. Functional connectivity MR imaging reveals cortical functional connectivity in the developing brain. Am. J. Neuroradiol. 29, 1883–1889. doi:10.3174/ajnr.a1256.

Liu, J., Liao, X., Xia, M., He, Y., 2018. Chronnectome fingerprinting: identifying individuals and predicting higher cognitive functions using dynamic brain connectivity patterns. Hum. Brain Mapp. 39, 902–915. doi:10.1002/hbm.23890.

Liu, J., Xia, M., Wang, X., Liao, X., He, Y., 2020. The spatial organization of the chronnectome associates with cortical hierarchy and transcriptional profiles in the human brain. Neuroimage 222, 117296. doi:10.1016/j.neuroimage.2020.117296.

Ma, L., Tian, L., Hu, T., Jiang, T., Zuo, N., 2021. Development of individual variability in brain functional connectivity and capability across the adult lifespan. Cereb. Cortex. doi:10.1093/cercor/bhab059.

Margulies, D.S., Ghosh, S.S., Goulas, A., Falkiewicz, M., Huntenburg, J.M., Langs, G., Bezgin, G., Eickhoff, S.B., Castellanos, F.X., Petrides, M., Jefferies, E., Smallwood, J., 2016. Situating the default-mode network along a principal gradient of macroscale cortical organization. Proc. Natl. Acad. Sci. U. S. A. 113, 12574–12579. doi:10.1073/pnas.1608282113.

Markello, R.D., Misic, B., 2021. Comparing spatial null models for brain maps. Neuroimage 236, 118052. doi:10.1016/j.neuroimage.2021.118052.

Ming, G., Song, H., 2011. Adult neurogenesis in the mammalian brain: significant answers and significant questions. Neuron 70, 687–702. doi:10.1016/j.neuron.2011.05.001.

Miranda-Dominguez, O., Feczko, E., Grayson, D.S., Walum, H., Nigg, J.T., Fair, D.A., 2018. Heritability of the human connectome: a connectotyping study. Netw. Neurosci. 02, 175–199. doi:10.1162/netn_a_00029.

Morgan, S.E., Seidlitz, J., Whitaker, K.J., Romero-Garcia, R., Clifton, N.E., Scarpazza, C., Amelsvoort, T.van, Marcelis, M., Os, J.van, Donohoe, G., Mothersill, D., Corvin, A., Pocklington, A., Raznahan, A., McGuire, P., Vértes, P.E., Bullmore, E.T., 2019. Cortical patterning of abnormal morphometric similarity in psychosis is associated with brain expression of schizophrenia-related genes. Proc. Natl. Acad. Sci. 116, 9604–9609. doi:10.1073/pnas.1820754116.

Mueller, S., Wang, D., Fox, M.D., Yeo, B.T.T., Sepulcre, J., Sabuncu, M.R., Shafee, R., Lu, J., Liu, H., 2013. Individual variability in functional connectivity architecture of the human brain. Neuron 77, 586–595. doi:10.1016/j.neuron.2012.12.028.

Paniukov, D., Lebel, R.M., Giesbrecht, G., Lebel, C., 2020. Cerebral blood flow increases across early childhood. Neuroimage 204, 116224. doi:10.1016/j.neuroimage.2019.116224.

Preti, M.G., Van De Ville, D., 2019. Decoupling of brain function from structure reveals regional behavioral specialization in humans. Nat. Commun. 10, 4747. doi:10.1038/s41467-019-12765-7.

Richiardi, J., Altmann, A., Milazzo, A.-.C., Chang, C., Chakravarty, M.M., Banaschewski, T., Barker, G.J., Bokde, A.L.W., Bromberg, U., Büchel, C., Conrod, P., Fauth-Bühler, M., Flor, H., Frouin, V., Gallinat, J., Garavan, H., Gowland, P., Heinz, A., Lemaître, H., Mann, K.F., Martinot, J.-.L., Nees, F., Paus, T., Pausova, Z., Rietschel, M., Robbins, T.W., Smolka, M.N., Spanagel, R., Ströhle, A., Schumann, G., Hawrylycz, M., Poline, J.-.B., Greicius, M.D., Consortium, I., 2015. Correlated gene expression supports synchronous activity in brain networks. Science 348, 1241–1244. doi:10.1126/science.1255905.

Romme, I.A., de Reus, M.A., Ophoff, R.A., Kahn, R.S., van den Heuvel, M.P., 2017. Connectome disconnectivity and cortical gene expression in patients with schizophrenia. Biol. Psychiatry 81, 495–502. doi:10.1016/j.biopsych.2016.07.012.

Satterthwaite, T.D., Shinohara, R.T., Wolf, D.H., Hopson, R.D., Elliott, M.A., Vandekar, S.N., Ruparel, K., Calkins, M.E., Roalf, D.R., Gennatas, E.D., Jackson, C., Erus, G., Prabhakaran, K., Davatzikos, C., Detre, J.A., Hakonarson, H., Gur, R.C., Gur, R.E., 2014. Impact of puberty on the evolution of cerebral perfusion during adolescence. Proc. Natl. Acad. Sci. 111, 8643–8648. doi:10.1073/pnas.1400178111.

Seidlitz, J., Váša, F., Shinn, M., Romero-Garcia, R., Whitaker, K.J., Vértes, P.E., Wagstyl, K., Kirkpatrick Reardon, P., Clasen, L., Liu, S., Messinger, A., Leopold, D.A., Fonagy, P., Dolan, R.J., Jones, P.B., Goodyer, I.M., Raznahan, A., Bullmore, E.T., 2018. Morphometric similarity networks detect microscale cortical organization and predict inter-individual cognitive variation. Neuron 97, 231–247.e7. doi:10.1016/j.neuron.2017.11.039, e7.

Smith, S.M., Nichols, T.E., Vidaurre, D., Winkler, A.M., Behrens, T.E.J., Glasser, M.F., Ugurbil, K., Barch, D.M., Van Essen, D.C., Miller, K.L., 2015. A positive-negative mode of population covariation links brain connectivity, demographics and behaviour. Nat. Neurosci. 18, 1565–1567. doi:10.1038/nn.4125.

Smyser, C.D., Inder, T.E., Shimony, J.S., Hill, J.E., Degnan, A.J., Snyder, A.Z., Neil, J.J., 2010. Longitudinal analysis of neural network development in preterm infants. Cereb. Cortex 20, 2852–2862. doi:10.1093/cercor/bhq035.

Stoecklein, S., Hilgendorff, A., Li, M., Förster, K., Flemmer, A.W., Galiè, F., Wunderlich, S., Wang, D., Stein, S., Ehrhardt, H., Dietrich, O., Zou, Q., Zhou, S., Ertl-Wagner, B., Liu, H., 2020. Variable functional connectivity architecture of the preterm human brain: impact of developmental cortical expansion and maturation. Proc. Natl. Acad. Sci. 117, 1201–1206. doi:10.1073/pnas.1907892117.

Tau, G.Z., Peterson, B.S., 2010. Normal development of brain circuits. Neuropsychopharmacology 35, 147–168. doi:10.1038/npp.2009.115.

Terracciano, A., Esko, T., Sutin, A.R., De Moor, M.H.M., Meirelles, O., Zhu, G., Tanaka, T., Giegling, I., Nutile, T., Realo, A., 2011. Meta-analysis of genome-wide association studies identifies common variants in CTNNA2 associated with excitement-seeking. Transl. Psychiatry 1. doi:10.1038/tp.2011.42, e49–e49.

Tzourio-Mazoyer, N., Landeau, B., Papathanassiou, D., Crivello, F., Etard, O., Delcroix, N., Mazoyer, B., Joliot, M., 2002. Automated anatomical labeling of activations in SPM using a macroscopic anatomical parcellation of the MNI MRI single-subject brain. Neuroimage 15, 273–289. doi:10.1006/nimg.2001.0978.

Van Essen, D.C., Smith, S.M., Barch, D.M., Behrens, T.E.J., Yacoub, E., Ugurbil, K., WU-Minn HCP Consortium, 2013. The WU-Minn human connectome project: an overview. Neuroimage 80, 62–79. doi:10.1016/j.neuroimage.2013.05.041.

Vértes, P.E., Rittman, T., Whitaker, K.J., Romero-Garcia, R., Váša, F., Kitzbichler, M.G., Wagstyl, K., Fonagy, P., Dolan, R.J., Jones, P.B., Goodyer, I.M., Consortium, N.S.P.N., Bullmore, E.T., 2016. Gene transcription profiles associated with inter-modular hubs and connection distance in human functional magnetic resonance imaging networks. Philos. Trans. R. Soc. Lond. B. Biol. Sci. 371. doi:10.1098/rstb.2015.0362.

Wang, D., Liu, H., 2014. Functional connectivity architecture of the human brain: not all the same. Neuroscientist 20, 432–438. doi:10.1177/1073858414543290.

Wang, G.-.Z., Belgard, T.G., Mao, D., Chen, L., Berto, S., Preuss, T.M., Lu, H., Geschwind, D.H., Konopka, G., 2015. Correspondence between resting-state activity and brain gene expression. Neuron 88, 659–666. doi:10.1016/j.neuron.2015.10.022.

Wei, Y., de Lange, S.C., Scholtens, L.H., Watanabe, K., Ardesch, D.J., Jansen, P.R., Savage, J.E., Li, L., Preuss, T.M., Rilling, J.K., Posthuma, D., van den Heuvel, M.P., 2019. Genetic mapping and evolutionary analysis of human-expanded cognitive networks. Nat. Commun. 10, 4839. doi:10.1038/s41467-019-12764-8.

Whitaker, K.J., Vértes, P.E., Romero-Garcia, R., Váša, F., Moutoussis, M., Prabhu, G., Weiskopf, N., Callaghan, M.F., Wagstyl, K., Rittman, T., Tait, R., Ooi, C., Suckling, J., Inkster, B., Fonagy, P., Dolan, R.J., Jones, P.B., Goodyer, I.M., Consortium, N.S.P.N., Bullmore, E.T., 2016. Adolescence is associated with genomically patterned consolidation of the hubs of the human brain connectome. Proc. Natl. Acad. Sci. U. S. A. 113, 9105–9110. doi:10.1073/pnas.1601745113.

Won, H., Huang, J., Opland, C.K., Hartl, C.L., Geschwind, D.H., 2019. Human evolved regulatory elements modulate genes involved in cortical expansion and neurodevelopmental disease susceptibility. Nat. Commun. 10, 2396. doi:10.1038/s41467-019-10248-3.

Yan, C., Zang, Y., 2010. DPARSF: a MATLAB toolbox for “pipeline” data analysis of resting-state fMRI. Front. Syst. Neurosci. 4. doi:10.3389/fnsys.2010.00013.

Yan, C.-.G., Wang, X.-.D., Zuo, X.-.N., Zang, .Y..-F., 2016. DPABI: data processing & analysis for (resting-state) brain imaging. Neuroinformatics 14, 339–351. doi:10.1007/s12021-016-9299-4.

Yarkoni, T., Poldrack, R.A., Nichols, T.E., Van Essen, D.C., Wager, T.D., 2011. Large-scale automated synthesis of human functional neuroimaging data. Nat. Methods 8, 665–670. doi:10.1038/nmeth.1635.

Yeo, B.T.T., Krienen, F.M., Sepulcre, J., Sabuncu, M.R., Lashkari, D., Hollinshead, M., Roffman, J.L., Smoller, J.W., Zöllei, L., Polimeni, J.R., Fischl, B., Liu, H., Buckner, R.L., 2011. The organization of the human cerebral cortex estimated by intrinsic functional connectivity. J. Neurophysiol. 106, 1125–1165. doi:10.1152/jn.00338.2011.

Zalesky, A., Fornito, A., Harding, I.H., Cocchi, L., Yücel, M., Pantelis, C., Bullmore, E.T., 2010. Whole-brain anatomical networks: does the choice of nodes matter? Neuroimage 50, 970–983. doi:10.1016/j.neuroimage.2009.12.027.